

Impact of Source to Drain Tunneling on the Ballistic Performance of Ge, GaSb, and GeSn Nanowire p-MOSFETs

Dibakar Yadav, Deleep R. Nair, *Member, IEEE*

Abstract—We investigated the effect of material choice and orientation in limiting source to drain tunneling (SDT) in nanowire (NW) p-MOSFETs. Si, Ge, GaSb, and Ge_{0.96}Sn_{0.04} nanowire MOSFETs (NWFETs) were simulated using rigorous ballistic quantum transport simulations. To properly account for the non-parabolicity and anisotropy of the valence band the k·p method was used. For each material, a set of six different transport/confinement directions were simulated to identify the direction with the highest ON-current (I_{ON}). For Ge, GaSb, and GeSn [001]/110/ $\bar{1}10$ oriented NWFETs showed the best ON-state performance, compared to other orientations. Our simulation results show that, despite having a higher percentage of SDT in OFF-state than silicon, GaSb [001]/110/ $\bar{1}10$ NWFET can outperform Si NWFETs. We further examined the role of doping in limiting SDT and demonstrated that the ON-state performance of Ge and GeSn NWFETs could be improved by reducing the doping in the source/drain (S/D) extension regions. Finally, we analyzed the impact of increased injection velocity in [001]/110/ $\bar{1}10$ oriented GaSb and GeSn NWFETs, as a result of the application of uniaxial compressive stress, and showed that when compared at a fixed OFF-current (I_{OFF}) with unstrained NWFETs, uniaxial compressive stress deteriorates the ON-state performance due to an increase in OFF-state SDT current component.

Index Terms—SDT, k·p method, Nanowire MOSFETs, Quantum transport simulations, NEGf, GaSb, GeSn.

I. INTRODUCTION

Increased SDT leakage in devices with short channel length can become a significant roadblock in scaling down transistor dimensions [1]–[3]. III-V semiconductors with high electron mobility like InGaAs, although regarded as promising candidates for future generation n-MOSFETs [4], are more susceptible to SDT leakage due to their lower transport effective mass (m_{trans}^*). III-V channel based p-MOSFETs can be more immune to SDT leakage in OFF-state compared to their n-channel counterparts, at scaled gate lengths due to their lower hole mobility (higher m_{trans}^*) compared to electron mobility [4]. Devices based on III-V materials like GaSb are being actively explored as a potential candidate to replace Si as a channel for the future generation of p-MOSFETs [5], [6]. At the same time, the anisotropic nature of the valence

band makes the performance of scaled p-MOSFET devices strongly dependent on the direction of transport/confinement [7]. Hence it may be possible to engineer hole effective masses in materials with higher hole mobility compared to Si, to limit SDT and improve the device performance. Germanium used to have the highest bulk hole mobility among all the elemental group IV and III-V semiconductors [4]. Recently, GeSn alloy based p-channel MOSFETs have achieved higher effective hole mobility compared to pure Ge based FETs [8], [9]. To enable device scaling with performance improvements over conventional Si-based p-MOSFETs, it is essential to explore the relative merits/demerits of MOSFETs based on alternate channel materials. Nanowire MOSFETs due to their ability to provide the ultimate electrostatic control of the channel by the gate are regarded as a promising device architecture to continue scaling [10]. Hence in this paper, we have carried out a comparative analysis of the ballistic performance of Ge, GaSb, and GeSn NWFETs, to determine their suitability as a channel material for the future generation of p-MOSFETs.

A lot of studies have focussed in assessing the performance of Si, Ge, and III-V nanowire n-MOSFETs in the presence of SDT [2], [11]–[13]. But a similar study involving III-V materials along with Si, Ge for nanowire p-MOSFETs has not been carried out. In [14], some III-V materials alongside Si, Ge NWs have been considered. The authors have focussed on the ability of these materials in blocking SDT current for n- and p-NWFETs, but ON-state performance of these materials have not been evaluated. Other studies involving nanowire p-MOSFETs have only considered Si and Ge as channel materials and have been carried out either at longer gate lengths [13], with smaller SDT current component or have employed a semiclassical top of the barrier (ToB) model [15], which doesn't account for SDT. In [7], [16] ballistic performance of Si NWFETs has been evaluated in different transport orientations using the ToB model. In [3] an optimized range of m^* has been provided, which has been treated as a material independent quantity, to optimize device performance for sub-12 nm nodes. In [3] however, transport was treated using a single band effective mass (EM) model. The EM model can't account for the non-parabolic and coupled nature of valence bands [17]. Recently, Chang et al. [18] have analyzed the ballistic performance of III-V double-gate p-MOSFETs using ToB semiclassical transport model.

In this work, we perform ballistic quantum transport simulations using the k·p method, to analyze the impact of SDT on

This paragraph of the first footnote will contain the date on which you submitted your paper for review.

D. Yadav and D. R. Nair are with Department of Electrical Engineering, IIT Madras, Chennai 600036, India (e-mail: dibakaryadav19@gmail.com; deleep@ee.iitm.ac.in).

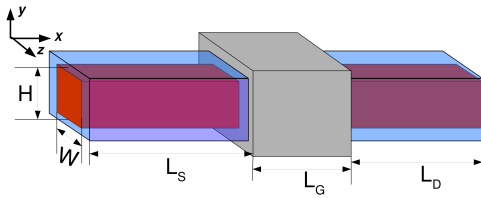


Fig. 1. Schematic of the simulation domain of nanowire MOSFETs used in this work.

the performance of nanowire p-MOSFETs. A comprehensive analysis of the effects of the valence band dispersion relations, resulting from the use of different channel materials and crystallographic orientations will provide essential guidelines in designing sub-10 nm p-MOSFETs. We have performed rigorous ballistic quantum transport simulations of NWFETs with Ge, GaSb, and GeSn as the channel materials and compared their performance with Si NWFETs. For these materials, we have attempted to identify the transport directions which can minimize the OFF-state SDT without compromising too much on the ON-state performance.

The rest of the paper is organized as follows. We briefly summarize the simulation approach in section II. In section III, we analyze the ballistic performance of all the four materials with different transport orientation, strain, and source/drain doping concentrations. We also investigate the behavior of injection velocity, quantum capacitance in the ballistic limit. Finally, we conclude the paper in section IV.

II. APPROACH

To investigate the effect of SDT on the performance of different channel materials, we adopt the following methodology,

- 1) All the materials have been compared at a fixed gate length of $L_G = 10$ nm. Dimensions of the NW cross-section are chosen to be $5 \text{ nm} \times 5 \text{ nm}$. Since our aim is to optimize m_{trans}^* to limit SDT, by varying channel material and orientation, rather than by changing device geometry, the dimensions of the device cross-section were kept constant throughout all the simulations.
- 2) We also analyzed the impact of channel transport orientation in minimizing SDT. For each material, NWFETs with six different transport orientations were simulated, to identify the orientation providing the highest I_{ON} . For a fair comparison, I_{OFF} for each orientation was made $100 \text{ nA}/\mu\text{m}$, by adjusting the gate work function.
- 3) The role of doping in minimizing SDT and improving I_{ON} has been examined for Ge and GeSn NWFETs.
- 4) Finally, for the directions with highest I_{ON} , we examined the impact of compressive stress, to determine whether any further increase in the ballistic injection velocity translates into higher I_{ON} for these devices.

We have solved self-consistently, the 3D-Poisson's equation and Schrödinger's equation within the non-equilibrium Green's function (NEGF) formalism, to analyze the effect of NW bandstructure and electrostatics on the overall performance of NWFETs. A schematic of NWFETs simulated in this study is shown in Fig. 1. For all the materials considered

TABLE I
SUMMARY OF NW AXIAL ORIENTATION AND DIRECTIONS OF CONFINEMENTS

NW axial orientation	Transport direction (x)	Confinement directions (y/z)
[100]	100	010/001
[110]	110	$\bar{1}10/001$
[111]	111	$0\bar{1}1/\bar{2}11$
[001]	001	$110/\bar{1}10$
$[0\bar{1}1]$	$0\bar{1}1$	$\bar{2}11/111$
$[\bar{2}11]$	$\bar{2}11$	$0\bar{1}1/111$

in this study, transport characteristics with [100]/010/001, [110]/ $\bar{1}10/110$, [111]/ $0\bar{1}1/\bar{2}11$, [001]/ $110/\bar{1}10$, $[0\bar{1}1]/\bar{2}11/111$, $[\bar{2}11]/0\bar{1}1/111$ orientations were simulated. The summary of NW transport directions simulated, with their directions of confinement is given in Table I. Hereafter, for brevity, we denote different NWs using their direction of transport. For materials with indirect bandgaps, the 6 band $k \cdot p$ method provides an accurate description of valence bands around the Γ point [19]. Hence for Si, Ge and GeSn, the 6 band $k \cdot p$ method has been used. For GaSb with a direct bandgap, we have used the 8 band $k \cdot p$ method.

To reduce the computational load associated with the solution of NEGF equations, we first transformed the device Hamiltonian from real space to reciprocal space [17]. Since the Hamiltonian in reciprocal space was still too expensive to be used in transport simulations, the mode-space (MS) Hamiltonian was constructed, which was then used in NEGF simulations. For the 6 band $k \cdot p$ method, the MS Hamiltonian was constructed following the approach outlined by Huang et al. in [20]. Similar to [20], we constructed the MS Hamiltonian by sampling the modes at the Γ point first (k-space sampling), and then by performing an energy space sampling at an energy of $E = E_{top} - E_{int}$, where E_{top} is the energy at the top of the valence band edge and E_{int} is the energy interval starting from E_{top} , over which we need the bandstructure obtained from the MS approach to match the bandstructure obtained using the reciprocal space Hamiltonian. The MS transformation Hamiltonian was then constructed by combining the modes obtained by k-space sampling to those obtained by energy space sampling and ortho-normalizing the resultant matrix [20]. For GaSb with the 8 band $k \cdot p$ model, the approach proposed in [21] was used. For 8 band $k \cdot p$ method, only k-space sampling was used [21]. Spurious energy states in the MS Hamiltonian were removed by discarding modes with singular values smaller than an iteratively determined threshold value [22]. For simulating NWs with different transport/surface orientations appropriate coordinate transformations were performed [23]. Recursive Green's function algorithm [24] was used to speed up the calculation of charge density. The converged charge density was then fed to a 3D Poisson's equation solver and these sequence of steps were repeated in a self-consistent manner.

To check the validity of MS transformation, we have compared the E-k relation obtained by using the MS Hamiltonian to the one obtained using the reciprocal-space Hamiltonian. The bandstructure of [100] oriented Si NW is shown in

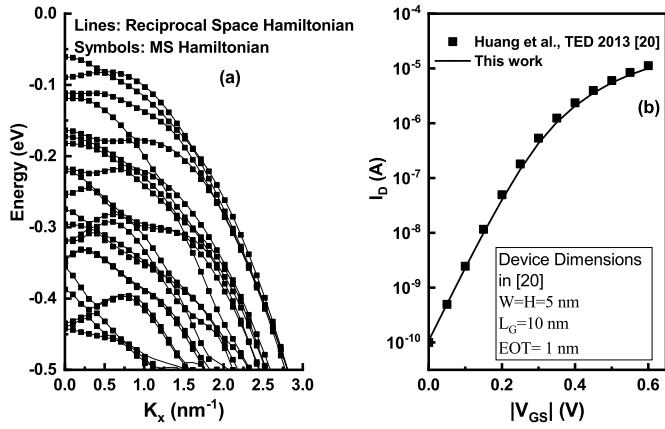


Fig. 2. (a) Hole subbands of Si [100] nanowire with 5 nm \times 5 nm area of cross-section, obtained from reciprocal space Hamiltonian (Solid lines) and mode space Hamiltonian (Symbols). (b) $I_D - V_{GS}$ characteristics for silicon NW pFET. Benchmarked results of Si NWFET to compare simulation approach. Our results (solid line) and [20] (symbols)

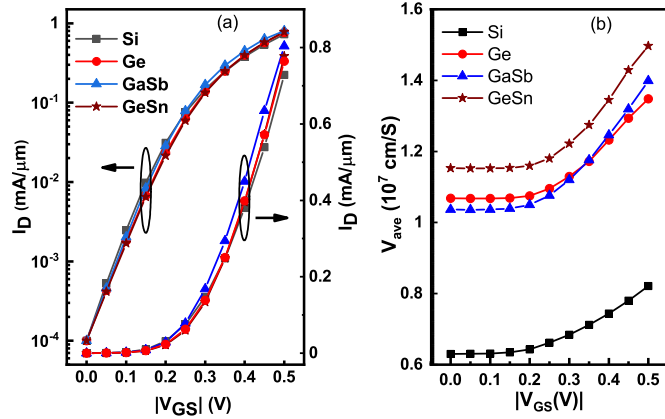


Fig. 3. (a) $I_D - V_{GS}$ characteristics of Si, Ge, GaSb and GeSn [100] oriented NWFETs. (b) V_{ave} at the virtual source for Si, Ge, GaSb and GeSn [100] oriented NWFETs.

Fig. 2(a). To benchmark the NEGF simulation approach, we performed simulations of a Si NWFET and compared it with a similar device in [20]; the results of benchmarking are shown in Fig. 2(b). The parameters used in simulation are given in Table II. Si parameters are taken from [25]. Luttinger parameters for Ge and Sn are taken from [26]. Elastic stiffness constants of GeSn are linearly interpolated from parameters of Ge and Sn [27]. Luttinger parameters of GaSb are taken from [22] and elastic stiffness constants from [18].

III. RESULTS AND DISCUSSION

The dimensions of the simulated devices are $L_S = L_D = 15$ nm. $L_G = 10$ nm. The dimensions of the cross-section are $W = H = 5$ nm. EOT of 0.6 nm and $V_{DD} = -0.5$ V were used in all simulations. Doping levels in S/D extension regions are 10^{20} cm $^{-3}$ for Si, Ge, and GeSn NWFETs, and 5×10^{19} cm $^{-3}$ for GaSb NWFETs.

A. Material Dependence

In this subsection, we compare the ballistic performance of [100] oriented NWFETs for all the four materials. Figure 3(a)

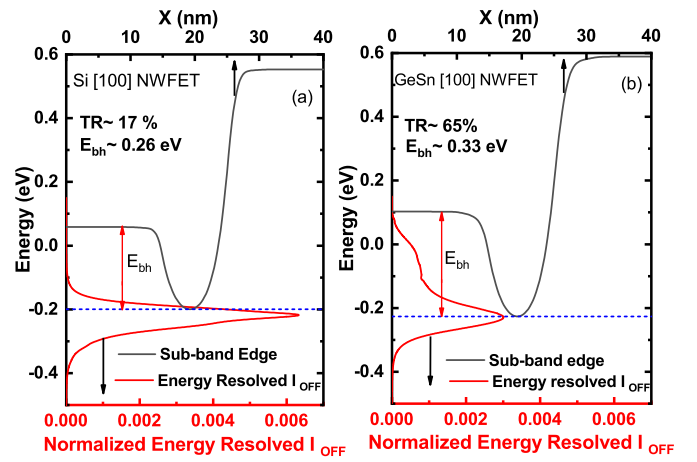


Fig. 4. Normalized current spectrum in OFF-state for (a) Si and (b) GeSn [100] oriented NWFETs. Currents values have been normalized by total I_{OFF} . Current flowing above the blue dashed lines constitutes the tunneling current.

TABLE II

LIST OF MATERIAL PARAMETERS USED IN SIMULATION. ONLY PARAMETERS NEEDED DURING SIMULATION ARE LISTED.

Parameters	Si	Ge	GaSb	GeSn
γ_1	3.60	9.37	13.27	10.54
γ_2	0.67	3.01	4.97	3.38
γ_3	1.21	4.02	5.978	4.52
Δ_{so} (eV)	0.044	0.306	0.748	0.332
m_c	–	–	0.042	–
E_g (eV)	–	–	0.751	–
E_p (eV)	–	–	21.2	–
a_c (eV)	–	–	-7.5	–
a_v (eV)	–	–	0.8	1.24
b (eV)	–	–	-2.0	-2.9
d (eV)	–	–	-4.7	-5.3
C_{11} (GPa)	–	–	88.5	123.72
C_{12} (GPa)	–	–	40.2	43.41
C_{44} (GPa)	–	–	43.2	65.77

shows the $I_D - V_{GS}$ characteristics of Si, Ge, GaSb and GeSn NWFETs oriented in [100] transport direction. Si NWFET has the lowest I_{ON} due to its lower injection velocity. Figure 3(b) shows the average ballistic injection velocity (V_{ave}) [28], [29] at the peak of the source-channel potential barrier. GeSn NWFET has the highest V_{ave} among all the four materials. It also has the highest component of SDT in the OFF-state. Figure 4 shows the normalized energy resolved I_{OFF} for Si and GeSn NWFETs in [100] orientation. For Si NWFET, tunnel ratio (TR) defined as the ratio of current flowing by tunneling to the total current in OFF-state is $\sim 17\%$. Thus most of the current in OFF-state is due to thermionic emission over the potential barrier. GeSn NWFET on the other hand has a TR of $\sim 65\%$, highest among all the four materials. Thus the potential barrier height (E_{bh}) needed to achieve the same I_{OFF} in [100] oriented GeSn NWFET is higher compared to [100] Si NWFET. This results in lower ON-state overdrive in [001] oriented GeSn NWFET.

GaSb [100] NWFET has the highest I_{ON} among all four materials. A lower TR $\sim 51\%$ for GaSb NWFET compared to GeSn results in a higher ON-state overdrive. GeSn NWFET

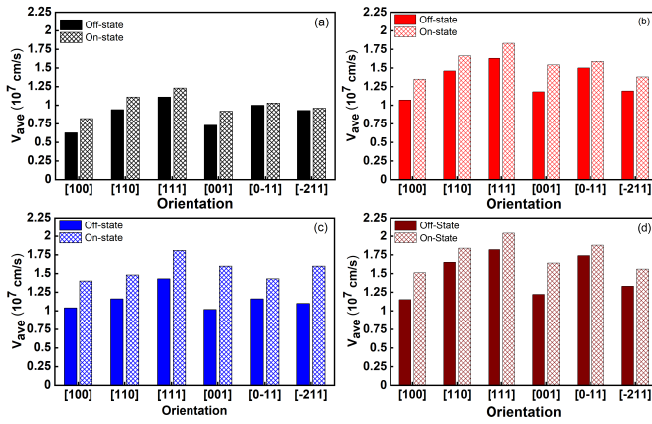


Fig. 5. ON and OFF-state V_{ave} at virtual source for (a) Si, (b) Ge, (c) GaSb, (d) GeSn NWFETs.

has the worst SS initially, due to higher TR, implying degraded gate control over the channel. But once the devices start operating above the sub-threshold region, the rise in current as V_{GS} increases, is steepest for GeSn NWFET. Reducing OFF-state tunneling by decreasing the doping concentration of S/D extension regions can counter the loss of ON-state overdrive. As shown in subsection III-C with similar S/D doping GeSn NWFET can outperform GaSb NWFET.

The performance of [100] oriented NWFETs is, however, sub-optimal in terms of I_{ON} . For all materials, an increase in the ballistic injection velocity, over its value in [100] oriented NWFETs results in an increased I_{ON} . However, for all materials I_{ON} doesn't increase proportionately, with an increase in injection velocity. The orientation dependent performance variation for all the materials is discussed in the next subsection.

B. Orientation Dependence

Table III shows I_{ON} for all materials with different orientations. Orientation dependence of V_{ave} at the virtual source is shown in Fig. 5. Both ON and OFF-state ballistic average injection velocities are shown. Irrespective of the material choice, [111] oriented NWFETs have the highest V_{ave} , while [100] oriented NWFETs has the lowest V_{ave} . Figure 6(a) shows the $I_D - V_{GS}$ characteristics of orientations with the highest ON-current for each material. In the case of Si NWFETs, [111] oriented NWFET has the highest I_{ON} . The superior performance of Si [111] oriented NWFET, which has the highest V_{ave} and TR among all Si NWFETs, shows that all Si NWFETs still operate in the thermionic current component dominated regime in OFF-state. For Ge, GaSb, and GeSn [001] oriented NWFETs have higher I_{ON} , compared to other orientations. The reason for the superior performance of [001] oriented NWFETs, over [100] oriented NWFETs is their very similar V_{ave} in OFF-state to [100] oriented NWFETs, as shown in Fig. 5. This results in [001] oriented NWFETs having similar TR and SS to [100] oriented NWFETs. In ON-state, however, the injection velocity for [001] oriented NWFETs is much higher compared to [100] orientation, thus resulting in better ON-state performance. In ON-state, as k-states with

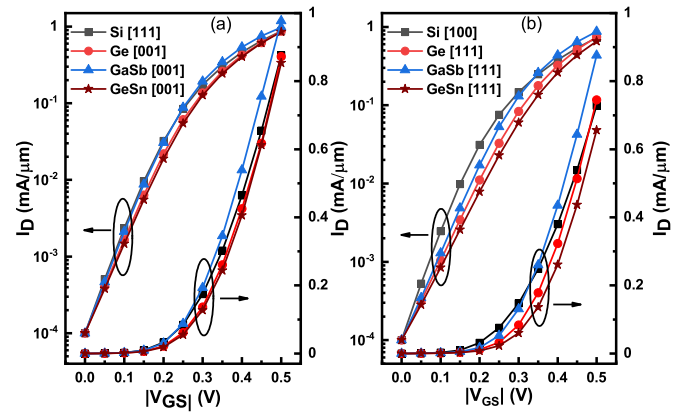


Fig. 6. (a) $I_D - V_{GS}$ characteristics for orientations with highest I_{ON} for each material. (b) Comparison of $I_D - V_{GS}$ characteristics of [111] oriented Ge, GaSb, and GeSn NWFETs with [100] Si NWFET.

TABLE III
 I_{ON} FOR Si, Ge, GaSb, AND GeSn NWFETs WITH DIFFERENT TRANSPORT ORIENTATION

Orientation	I_{ON} (mA/ μ m)			
	Si	Ge	GaSb	GeSn
100/010/001	0.73	0.76	0.80	0.78
110/ $\bar{1}$ 10/001	0.84	0.74	0.80	0.69
111/0 $\bar{1}$ 1/211	0.88	0.75	0.88	0.66
001/110/ $\bar{1}$ 10	0.80	0.87	0.98	0.85
0 $\bar{1}$ 1/ $\bar{2}$ 11/111	0.80	0.70	0.82	0.62
$\bar{2}$ 11/0 $\bar{1}$ 1/111	0.82	0.72	0.85	0.62

higher energy, farther away from the Brillouin zone center are occupied, V_{ave} increases. These states have higher velocity compared to states near the $k = 0$ point [28], due to the higher gradient of the dispersion relation for off-zone center states. The gradient of energy with respect to k for [001] oriented NWs for Ge, GaSb, and GeSn is much higher compared to [100] oriented NWFETs. Hence once the high energy off-zone centre states are populated in ON-state, V_{ave} increases significantly for [001] NWFETs.

For [111] oriented NWFETs, the larger injection velocity (lower m_{trans}^*) results in higher SDT, and degraded gate control. Figure 6(b) shows the $I_D - V_{GS}$ characteristics of [111] oriented NWFETs, for Ge, GaSb and GeSn NWs. $I_D - V_{GS}$ characteristic of Si [100] NWFET, which has the lowest V_{ave} in ON and OFF-states is also shown for comparison. The degraded gate control and higher SS for [111] NWs results in them showing much inferior performance in the sub-threshold region. The SS for the first decade of change in I_D from the I_{OFF} value, and TR for different materials and transport direction combinations, is given in Table IV. As can be seen, for all the materials [111] oriented NWFETs have the worst SS and highest TR. Higher V_{ave} for [111] oriented NWFETs is not enough to compensate for the loss of ON-state overdrive due to higher SDT in OFF-state. Hence [111] oriented Ge, GaSb, and GeSn NWFETs underperform compared to [001] oriented NWFETs for these materials.

For comparison across materials, we show the quantum capacitance (QC) [30] as a function of V_{GS} in Fig. 7(a) for Si

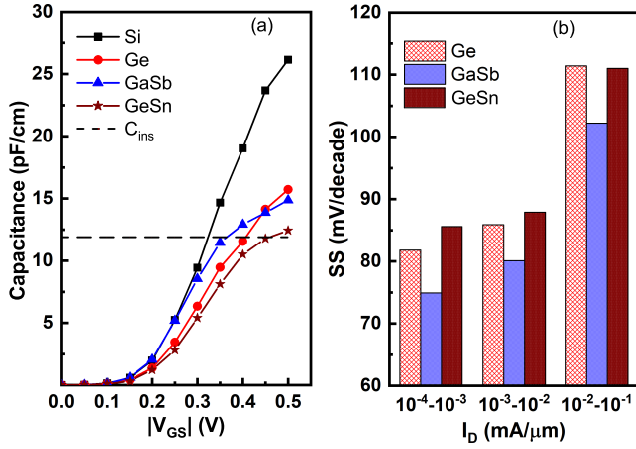


Fig. 7. (a) Quantum capacitance vs Gate voltage for directions with highest ON-current for each material. (b) SS for first 3 decades of I_D for [001] oriented Ge, GaSb and GeSn NWFETs.

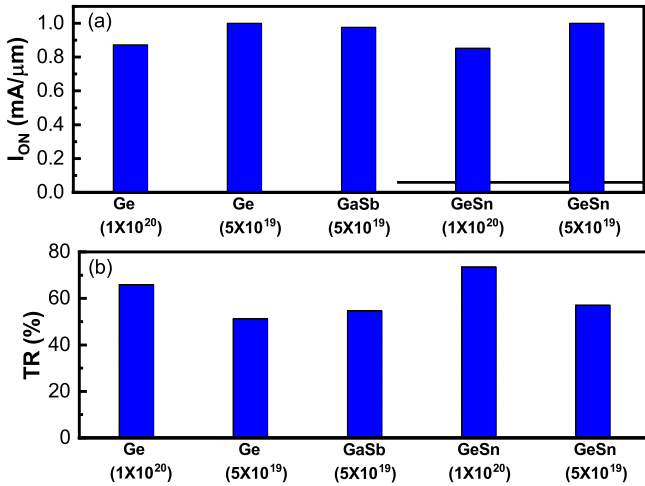


Fig. 8. (a) Doping dependence of I_{ON} for Ge and GeSn [001] oriented NWFETs. I_{ON} for [001] oriented GaSb NWFET is also shown for comparison. (b) Tunnel ratios for devices considered in (a). Doping levels in S/D extension regions in cm^{-3} are indicated within brackets.

[111] and [001] oriented Ge, GaSb, and GeSn NWFETs. These are the directions having the highest I_{ON} for each material. Our simulation results show that these devices operate in the classical capacitance regime [30]. Hence the QC is greater than the NW insulator capacitance (C_{ins}) [31]. Ge and GaSb [001] oriented NWFETs have comparable values of QC and V_{ave} (as shown in Fig. 5). Despite this, GaSb [001] NWFET outperforms Ge [001] oriented NWFET and has the highest I_{ON} among all materials, with all different orientations considered. Ge [001] oriented NWFETs underperform compared to GaSb [001] oriented NWFETs primarily due to higher OFF-state SDT and worse SS. Figure 7(b) shows the SS over the first three decades of I_D , over which the characteristics are sub-threshold like. Ge [001] NWFET has higher SS in this region due to degraded gate control as a result of higher SDT. Higher SDT in Ge [001] NWFET compared to GaSb [001] oriented NWFET is partly also due to the higher doping in the S/D extension regions. SDT can be reduced by reducing the doping in S/D extension regions [32]. With the same level

TABLE IV

SS AND TR FOR Si, Ge, GaSb, AND GeSn NWFETs WITH DIFFERENT TRANSPORT ORIENTATIONS

Material and Orientation	SS (mV/dec)	TR
Si [100]	70	16.64%
Si [111]	72	39.76%
Ge [001]	82	65.97%
Ge [111]	99	91.24%
GaSb [001]	75	54.69%
GaSb [111]	90	86.23%
GeSn [001]	86	73.39%
GeSn [111]	108	95.86%

of doping as GaSb, both Ge and GeSn NWFETs outperform [001] GaSb NWFETs, as shown in the next subsection.

C. Impact of Doping and Strain

In this subsection, we reduce the doping levels in the S/D extension regions of Ge and GeSn NWFETs from 1×10^{20} to $5 \times 10^{19} \text{ cm}^{-3}$, to compare their performance with GaSb NWFETs at the same level of doping. [001] oriented NWFETs were simulated as they provide the highest I_{ON} for each of the three materials. Figure 8(a) shows I_{ON} for [001] oriented Ge and GeSn NWFETs with S/D doping of $5 \times 10^{19} \text{ cm}^{-3}$ and $1 \times 10^{20} \text{ cm}^{-3}$. At the same value of S/D doping, Ge and GeSn NWFETs show marginally better ON-state performance as compared to GaSb [001] oriented NWFET. The TRs for these devices is shown in Fig. 8(b). Tunnel ratios improve considerably for both Ge and GeSn [001] oriented NWFETs at lower doping levels. Reduction of S/D doping leads to lower SDT and improved SS. The impact of lower S/D doping on V_{ave} at the virtual source is shown in Fig. 9. The OFF-state V_{ave} remains practically unchanged for lower doping levels in the S/D extension regions. Hence, the reduction in SDT is due to the widening of source-channel potential as a result of lower doping levels in S/D extension regions [33]. The ON-state V_{ave} increases slightly, primarily due to enhanced ON-state overdrive voltage, which results in hole sub-bands moving more closer to the source contact Fermi level, thus increasing the occupation probability of the sub-bands.

Finally, we have also examined the impact of compressive stress on the performance of GaSb and GeSn [001] oriented NWFETs, to determine whether any further increase in the injection velocity due to strain, benefits the ON-state performance. Ge [001] NWFET has not been considered as it has similar value of I_{ON} , elastic constants, and deformation potentials as GeSn [001] NWFET. Our simulation results show that ON-state performance deteriorates due to uniaxial compressive stress. Figure 10 shows the $I_D - V_{GS}$ characteristics of GaSb and GeSn [001] NWFETs with 1 GPa compressive stress along transport direction, the $I_D - V_{GS}$ characteristics of GaSb and GeSn [001] unstrained NWFETs is also shown for comparison. OFF-state SDT is enhanced due to uniaxial compressive stress, resulting in inferior ON-state performance. Unlike the case of reduced doping, the OFF-state V_{ave} is increased due to compressive stress, which results in higher SDT in OFF-state. Average ballistic injection velocity as a function of V_{GS}

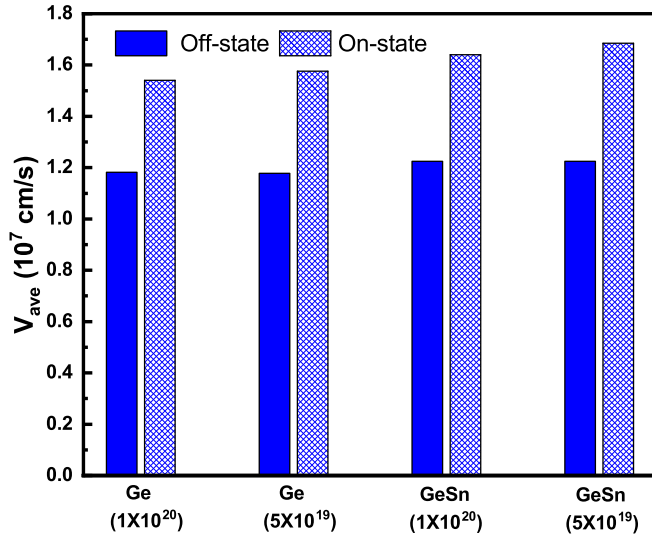


Fig. 9. (a) Doping dependence of ON and OFF-state V_{ave} at the virtual source for [001] oriented Ge and GeSn NWFETs having two different doping levels in S/D extension regions.

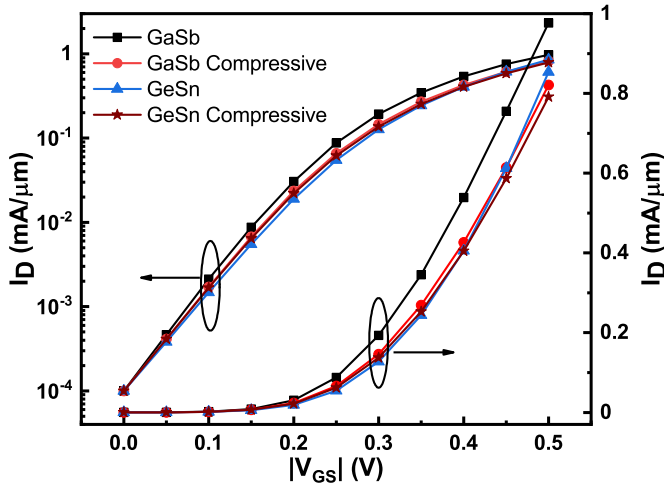


Fig. 10. (a) I_D - V_{GS} characteristics of [001] oriented GaSb and GeSn NWFETs with and without uniaxial compressive stress of 1 GPa.

is shown in Fig. 11(a) for both GeSn and GaSb NWFETs with and without applied compressive stress. As can be seen, the OFF-state V_{ave} increases significantly for compressively strained GeSn and GaSb NWFETs, resulting in increased SDT. Figure 11(b) shows the inversion charge density at the virtual source for strained and unstrained GaSb and GeSn NWFETs. The inversion density is also slightly reduced due to compressive stress. Thus any further injection velocity enhancement doesn't result in better ON-state performance at this gate length, when compared at a fixed I_{OFF} .

IV. CONCLUSION

In summary, we have studied the effectiveness of material choice and orientation as handles to counter SDT in OFF-state. Our simulation results show that,

- 1) At $L_G = 10$ nm, all Si NWFETs have SDT current component $< 50\%$ in OFF-state. Among all Si NWFETs,

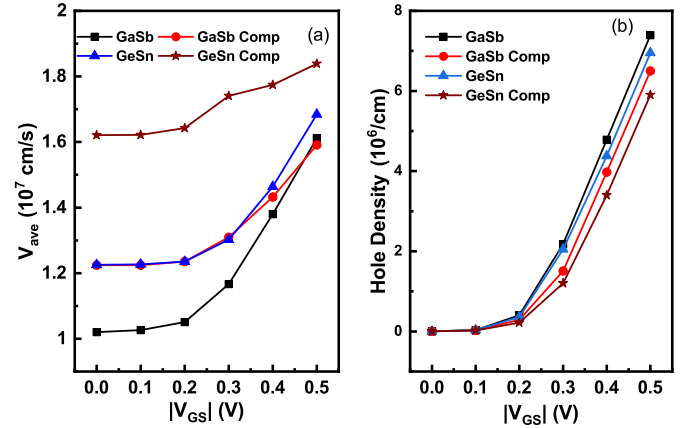


Fig. 11. (a) v_{ave} at the virtual source of [001] oriented GaSb and GeSn NWFETs with and without uniaxial compressive stress. (b) Inversion charge density at the virtual source for devices considered in (a).

[111] oriented NWFET with highest V_{ave} shows the best ON-state performance.

- 2) Other materials operate in the tunneling current dominated regime in OFF-state ($TR > 50\%$). For Ge, GaSb and GeSn, [001] oriented NWFETs with V_{ave} lying between that of [100] and [111] orientation for each material, show the best ON-state performance.
- 3) GaSb [001] oriented NWFET shows the best ON-state performance, among all the materials with all six different transport orientations considered. This is true, when Ge and GeSn NWFETs have higher doping concentration in S/D extension regions. At the same level of doping; however, [001] oriented Ge and GeSn NWFETs perform slightly better as compared to GaSb NWFET with the same orientation.
- 4) Finally, our simulation results show that any further enhancement in the injection velocity for [001] oriented NWFETs with GaSb and GeSn as the channel materials, by the application of uniaxial compressive stress doesn't result in better ON-state performance when compared at a fixed I_{OFF} . In fact, due to increased SDT in OFF-state, I_{ON} is reduced in [001] oriented NWFETs with uniaxial compressive stress.

We note here that the impact of the NW cross-section dimensions, on the device performance, has not been considered in this work. For NWs with smaller cross-section, atomistic tight binding (TB) method will be more accurate compared to the continuum based $k \cdot p$ method. For them, the modespace transformation of the TB Hamiltonian [34] can also be performed at a relatively cheaper computational cost. The impact of NW cross-section dimension and gate length on these set of channel materials will be the subject of a future study. While in this work, we have not considered the effects of phonon and surface roughness scattering and alloy scattering for GeSn NWFETs, the current study can nonetheless provide useful guidelines in the selection of materials and orientations, so as to minimize the effect of SDT in nanowire p-MOSFETs.

REFERENCES

- [1] J. Wang and M. Lundstrom, "Does source-to-drain tunneling limit the ultimate scaling of MOSFETs?" in *Digest. International Electron Devices Meeting.*, Dec 2002, pp. 707–710, doi: 10.1109/IEDM.2002.1175936.
- [2] S. R. Mehrotra, S. Kim, T. Kubis, M. Povolotskyi, M. S. Lundstrom, and G. Klimeck, "Engineering nanowire n-MOSFETs at $L_g < 8\text{nm}$," *IEEE Transactions on Electron Devices*, vol. 60, no. 7, pp. 2171–2177, July 2013, doi: 10.1109/TED.2013.2263806.
- [3] M. Salmani-Jelodar, S. R. Mehrotra, H. Ilatikhameneh, and G. Klimeck, "Design guidelines for sub-12 nm nanowire MOSFETs," *IEEE Transactions on Nanotechnology*, vol. 14, no. 2, pp. 210–213, March 2015, doi: 10.1109/TNANO.2015.2395441.
- [4] J. A. Del Alamo, "Nanometre-scale electronics with III–V compound semiconductors," *Nature*, vol. 479, pp. 317–323, Nov. 2011, doi: 10.1038/nature10677.
- [5] A. W. Dey, J. Svensson, B. M. Borg, M. Ek, and L.-E. Wernersson, "Single InAs/GaSb nanowire low-power CMOS inverter," *Nano Letters*, vol. 12, no. 11, pp. 5593–5597, Oct 2012, pMID: 23043243. [Online]. Available: <https://doi.org/10.1021/nl302658y>
- [6] A. Nainani, T. Irisawa, Z. Yuan, B. R. Bennett, J. B. Boos, Y. Nishi, and K. C. Saraswat, "Optimization of the $\text{Al}_2\text{O}_3/\text{GaSb}$ interface and a high-mobility GaSb pMOSFET," *IEEE Transactions on Electron Devices*, vol. 58, no. 10, pp. 3407–3415, Oct 2011, doi: 10.1109/TED.2011.2162732.
- [7] S. Mehrotra, A. Paul, M. Luisier, and G. Klimeck, "Surface and orientation dependence on performance of trigated silicon nanowire pMOSFETs," in *2009 IEEE Workshop on Microelectronics and Electron Devices*, April 2009, pp. 1–4, doi: 10.1109/WMED.2009.4816145.
- [8] G. Han, S. Su, C. Zhan, Q. Zhou, Y. Yang, L. Wang, P. Guo, W. Wei, C. P. Wong, Z. X. Shen, B. Cheng, and Y. Yeo, "High-mobility germanium-tin (GeSn) P-channel MOSFETs featuring metallic source/drain and sub-370 °c process modules," in *2011 International Electron Devices Meeting*, Dec 2011, pp. 16.7.1–16.7.3, doi: 10.1109/IEDM.2011.6131569.
- [9] S. Gupta, R. Chen, B. Magyari-Kope, H. Lin, B. Yang, A. Nainani, Y. Nishi, J. S. Harris, and K. C. Saraswat, "GeSn technology: Extending the Ge electronics roadmap," in *2011 International Electron Devices Meeting*, Dec 2011, pp. 16.6.1–16.6.4, doi: 10.1109/IEDM.2011.6131568.
- [10] K. J. Kuhn, "Considerations for ultimate CMOS scaling," *IEEE Transactions on Electron Devices*, vol. 59, no. 7, pp. 1813–1828, July 2012, doi: 10.1109/TED.2012.2193129.
- [11] R. Kim, U. E. Avci, and I. A. Young, "Comprehensive performance benchmarking of III-V and Si nMOSFETs (Gate Length = 13 nm) considering supply voltage and off-current," *IEEE Transactions on Electron Devices*, vol. 62, no. 3, pp. 713–721, March 2015, doi: 10.1109/TED.2015.2388708.
- [12] M. Luisier, M. Lundstrom, D. A. Antoniadis, and J. Bokor, "Ultimate device scaling: Intrinsic performance comparisons of carbon-based, InGaAs, and Si field-effect transistors for 5 nm gate length," in *2011 International Electron Devices Meeting*, Dec 2011, pp. 11.2.1–11.2.4, doi: 10.1109/IEDM.2011.6131531.
- [13] R. Kim, U. E. Avci, and I. A. Young, "CMOS performance benchmarking of Si, InAs, GaAs, and Ge nanowire n- and pMOSFETs with $L_g=13$ nm based on atomistic quantum transport simulation including strain effects," in *2015 IEEE International Electron Devices Meeting (IEDM)*, Dec 2015, pp. 34.1.1–34.1.4, doi: 10.1109/IEDM.2015.7409824.
- [14] S. S. Sylvia, H. Park, M. A. Khayer, K. Alam, G. Klimeck, and R. K. Lake, "Material selection for minimizing direct tunneling in nanowire transistors," *IEEE Transactions on Electron Devices*, vol. 59, no. 8, pp. 2064–2069, Aug 2012, doi: 10.1109/TED.2012.2200688.
- [15] J. Wang, A. Rahman, G. Klimeck, and M. Lundstrom, "Bandstructure and orientation effects in ballistic Si and Ge nanowire FETs," in *IEEE International Electron Devices Meeting, 2005. IEDM Technical Digest.*, Dec 2005, pp. 4 pp.–533, doi: 10.1109/IEDM.2005.1609399.
- [16] N. Neophytou, S. G. Kim, G. Klimeck, and H. Kosina, "On the bandstructure velocity and ballistic current of ultra-narrow silicon nanowire transistors as a function of cross section size, orientation, and bias," *Journal of Applied Physics*, vol. 107, no. 11, pp. 113 701–1–113 701–9, June 2010, doi: 10.1063/1.3372764. [Online]. Available: <https://doi.org/10.1063/1.3372764>
- [17] M. Shin, "Full-quantum simulation of hole transport and band-to-band tunneling in nanowires using the $k \cdot p$ method," *Journal of Applied Physics*, vol. 106, no. 5, pp. 054 505–1–054 505–10, Sept 2009, doi: 10.1063/1.3208067. [Online]. Available: <https://doi.org/10.1063/1.3208067>
- [18] P. Chang, X. Liu, S. Di, and G. Du, "Evaluation of ballistic transport in III–V-based p-Channel MOSFETs," *IEEE Transactions on Electron Devices*, vol. 64, no. 3, pp. 1053–1059, March 2017, doi: 10.1109/TED.2017.2655261.
- [19] C. Martinez-Blanco, E. G. Marin, A. Toral, J. M. Gonzalez-Molina, F. G. Ruiz, A. Godoy, and F. Gámiz, "Electrostatic performance of InSb, GaSb, Si and Ge p-channel nanowires," *Journal of Physics D: Applied Physics*, vol. 50, no. 49, p. 495106, 2017. [Online]. Available: <http://stacks.iop.org/0022-3727/50/i=49/a=495106>
- [20] J. Z. Huang, W. C. Chew, J. Peng, C. Yam, L. J. Jiang, and G. Chen, "Model order reduction for multiband quantum transport simulations and its application to p-type junctionless transistors," *IEEE Transactions on Electron Devices*, vol. 60, no. 7, pp. 2111–2119, July 2013, doi: 10.1109/TED.2013.2260546.
- [21] J. Z. Huang, L. Zhang, W. C. Chew, C. Yam, L. J. Jiang, G. Chen, and M. Chan, "Model order reduction for quantum transport simulation of band-to-band tunneling devices," *IEEE Transactions on Electron Devices*, vol. 61, no. 2, pp. 561–568, Feb 2014, doi: 10.1109/TED.2013.2295983.
- [22] J. Z. Huang, L. Zhang, P. Long, M. Povolotskyi, and G. Klimeck, "Quantum transport simulation of III-V TFETs with reduced-order $k \cdot p$ method," *ArXiv e-prints*, Nov. 2015. [Online]. Available: <http://adsabs.harvard.edu/abs/2015arXiv151102516H>
- [23] D. Esseni, P. Palestri, and L. Selmi, *Nanoscale MOS Transistors: Semi-Classical Transport and Applications*. Cambridge University Press, 2011, doi: 10.1017/CBO9780511973857.
- [24] D. Nikonov and S. Koswatta, "Recursive algorithm for NEGF in Matlab," Nov 2006. [Online]. Available: <https://nanohub.org/resources/1983>
- [25] M. Shin, S. Lee, and G. Klimeck, "Computational study on the performance of Si nanowire pMOSFETs based on the $k \cdot p$ method," *IEEE Transactions on Electron Devices*, vol. 57, no. 9, pp. 2274–2283, Sept 2010, doi: 10.1109/TED.2010.2052400.
- [26] S. Gupta, V. Moroz, L. Smith, Q. Lu, and K. C. Saraswat, "7-nm FinFET CMOS design enabled by stress engineering using Si, Ge, and Sn," *IEEE Transactions on Electron Devices*, vol. 61, no. 5, pp. 1222–1230, May 2014, doi: 10.1109/TED.2014.2311129.
- [27] H. Wang, Y. Liu, G. Han, Y. Shao, C. Zhang, Q. Feng, J. Zhang, and Y. Hao, "Performance enhancement in uniaxially strained Germanium–Tin FinTFET: Fin direction dependence," *IEEE Transactions on Electron Devices*, vol. 64, no. 7, pp. 2804–2811, July 2017, doi: 10.1109/TED.2017.2706559.
- [28] J. T. Teherani, "A comprehensive theoretical analysis of hole ballistic velocity in Si, SiGe, and Ge: Effect of uniaxial strain, crystallographic orientation, body thickness, and gate architecture," *IEEE Transactions on Electron Devices*, vol. 64, no. 8, pp. 3316–3323, Aug 2017, doi: 10.1109/TED.2017.2708691.
- [29] S. Zhang, J. Z. Huang, A. Khaliq, H. Xie, W. Chen, and W. Yin, "Quantum transport study of Si ultrathin-body double-gate pMOSFETs: $I - V$, $C - V$, energy delay, and parasitic effects," *IEEE Transactions on Electron Devices*, vol. 66, no. 1, pp. 655–663, Jan 2019, doi: 10.1109/TED.2018.2881160.
- [30] M. A. Khayer and R. K. Lake, "The quantum and classical capacitance limits of InSb and InAs nanowire FETs," *IEEE Transactions on Electron Devices*, vol. 56, no. 10, pp. 2215–2223, Oct 2009, doi: 10.1109/TED.2009.2028401.
- [31] I. Tienda-Luna, F. G. Ruiz, L. Donetti, A. Godoy, and F. Gámiz, "Modeling the equivalent oxide thickness of surrounding gate SOI devices with high- κ insulators," *Solid-State Electronics*, vol. 52, no. 12, pp. 1854 – 1860, 2008, selected Papers from the EUROSIOI '08 Conference. [Online]. Available: <http://www.sciencedirect.com/science/article/pii/S0038110108003080>
- [32] R. Kim, U. E. Avci, and I. A. Young, "Source/drain doping effects and performance analysis of ballistic III-V n-MOSFETs," *IEEE Journal of the Electron Devices Society*, vol. 3, no. 1, pp. 37–43, Jan 2015, doi: 10.1109/JEDS.2014.2363389.
- [33] M. Salmani Jelodar, H. Ilatikhameneh, P. Sarangapani, S. R. Mehrotra, G. Klimeck, S. Kim, and K. Ng, "Tunneling: The major issue in ultra-scaled MOSFETs," in *2015 IEEE 15th International Conference on Nanotechnology (IEEE-NANO)*, July 2015, pp. 670–673, doi: 10.1109/NANO.2015.7388694.
- [34] G. Mil'nikov, N. Mori, and Y. Kamakura, "Equivalent transport models in atomistic quantum wires," *Phys. Rev. B*, vol. 85, pp. 035 317–1–035 317–11, Jan 2012. [Online]. Available: <https://link.aps.org/doi/10.1103/PhysRevB.85.035317>